

# Dipolar solvent contributions for transient nanoscale electroosmotic flow

Pramodt Srinivasula\*

*ElectroSoft Labs LLP, Mumbai, India*

(\*pramodt.research@gmail.com)

(Dated: March 16, 2026)

Electrohydrodynamic flows of weak electrolytes at the nanoscale are significantly influenced by the molecular structure of water-like polar solvents within the electric double layer (EDL). Moreover, unlike in microfluidics, at these length scales the time scale of evolution of EDL often becomes comparable to the consequent fluidic phenomena of interest. While continuum descriptions to model such phenomena typically assume a constant dielectric and viscous solvent background, this study incorporates dipolar solvent physics, specifically both dielectric saturation and the viscoelectric effect together, into a Poisson-Nernst-Planck-Stokes (PNP-S) framework, using the Langevin-Bikerman solvent permittivity distribution and empirical viscoelectric coefficients, respectively. Numerical simulations in a one-dimensional geometry reveal substantial modifications to the electrohydrodynamic body force density and transient electroosmotic mobility during EDL evolution. The magnitude and temporal evolution of these corrections are characterized across parametric regimes, revealing systematic departures from standard constant-permittivity and constant-viscosity models, with electroosmotic mobility reductions of up to 50% governed by a characteristic dimensionless parameter. The results provide a solvent-consistent continuum framework for transient nanoscale electroosmotic flows and quantify the impact of molecular solvent structure on electrohydrodynamic transport relevant to modern nanofluidic applications.

## I. INTRODUCTION

Recent advances in nanofluidic and nanopore-based technologies, most prominently in ionic logic devices [1], DNA sequencing [2] and energy harvesting [3] have brought renewed attention to electrohydrodynamic (EHD) transport at nanometer length scales. In such systems, transport is governed by the formation and evolution of electric double layers (EDLs), whose characteristic length and time scales are comparable to the confinement scale and the timescales of the imposed electrohydrodynamic forcing. As a result, unlike microfluidic systems, transient electrokinetic phenomena rather than steady-state responses often control device performance.

Time-dependent EDL dynamics play a central role in modern nanofluidic applications. In voltage-gated nanopores and nanofluidic transistors, externally applied potentials actively modulate ionic transport by dynamically reshaping the EDL structure [4–7]. Similar transient processes influence signal resolution and noise characteristics in nanopore-based biosensing and sequencing, where electroosmotic flow (EOF) couples directly to ionic current fluctuations [8–10]. Beyond biosensing, transient EHD effects are also essential in shock electro dialysis [11], electroconvective transport in nanoporous membranes [12, 13], and energy-conversion devices employing confined electrolytes.

These systems are typically driven by pulsed or time-varying voltages and operate in geometries with extreme aspect ratios (with one of the lengths ranging up to  $0.1\ \mu\text{m}$  while some others as low as 10 nm), rendering direct experimental resolution and molecular simulation challenging. Consequently, continuum models remain indispensable for describing their dynamics [14]. Despite the central role of fluid motion, ionic transport, and electrokinetic coupling in these systems, their treatment from a fluid-mechanical perspective has been comparatively limited. Such studies emphasized more on the steady-state behavior, even while Poisson–Nernst–Planck and Navier–Stokes coupled frameworks were employed to model ionic transport and electroosmosis in the recent nanopores research [1–3, 15–18], with limited attention to transient hydrodynamic responses.

More importantly, at the nanoscale, electrokinetic behavior often departs from classical microfluidic scaling [19]. Experiments have reported enhanced EOF velocities, anomalously large electrostatic pressures, and increased energy conversion efficiencies in nanochannels and nanopores, signaling missing physics in traditional Poisson–Boltzmann-based models [19, 20]. To address these discrepancies, continuum theories have progressively incorporated molecular-scale corrections. Steric effects are commonly introduced via lattice-gas (Such as Bikerman) model [21, 22] or interacting hard-spheres (such as BMCSL) formalisms [23], while ion–solvent interactions are modeled through dielectrophoretic forces on solvated ions, Born energy variations [23]. These generally enhance EOF, while electroviscous and viscoelectric effects tend to suppress it [23–25]. More costly approaches involving immersed particles methods were also developed to capture the discrete ion-solvent interactions [26]. However, many of these approaches remain focused on the highly concentrated electrolytes while retaining a spatially uniform background permittivity of the solvent, implicitly neglecting the dipolar nature of the pure solvent, especially relevant for the low and moderately concentrated electrolytes.

---

\* Previously at the Department of Mechanical Engineering, TU Darmstadt, Germany, where part of the research was conducted.

It is now well established that solvent dipolar polarization plays a decisive role in nanoscale electrostatics. Direct measurements [27] and MD simulations [28] have demonstrated strong dielectric saturation of water near charged surfaces, with the effective permittivity decreasing dramatically under high electric fields. Continuum models incorporating dipolar solvents, most notably Langevin–Bikerman (LB) and related Landau-type formulations [29, 30], have successfully captured steady-state dielectric saturation and excluded-volume effects within the EDL. These models predict modified potential distributions, altered electrostatic pressures, and renormalized ion distributions [29, 31]. Despite this progress, their extension to transient electrohydrodynamic phenomena, particularly electroosmotic flow and other fluidic aspects, remains limited.

Multiple recent efforts have sought to embed dipolar solvent physics into generalized PNP frameworks, with the field-dependent polarization density and permittivity [32–34]. While theoretically rich, such models often lead to higher order, strongly nonlinear governing equations that are numerically stiff and difficult to integrate with hydrodynamic solvers. As a result, such approaches are currently limited to mathematical formulations and subsequent applications have been restricted to steady-state ion transport or rarely to steady-state EOF [35]. Robust numerical implementations of such solvent-dependent formulations for time-dependent EOF and fluid stresses has not been systematically explored.

A parallel but largely independent body of works in the literature concerns the viscoelectric effect, the increase of liquid viscosity under strong electric fields due to dipolar reorientation. Originally identified in polar organic liquids [36, 37] and later extrapolated to water [38, 39], the viscoelectric effect is commonly modeled through an empirical quadratic dependence of viscosity on electric field strength. Modern surface-force-balance experiments have recently confirmed the magnitude of this effect in water [40], validating decades-old estimates. Nevertheless, in most electrokinetic models, viscoelectricity is treated as a secondary, near-wall correction and is rarely examined in conjunction with dielectric saturation or transient EDL dynamics. At nanometer confinement, where electric fields are large and the flow is strongly coupled to the EDL, this separation is no longer justified.

Electroosmotic mobility in nanochannels emerges from the coupled evolution of charge density and electric field dependent solvent permittivity, viscous stress within the EDL. Steady-state studies have shown that incorporating dielectric saturation can substantially modify EOF mobility, while viscoelectric effects tend to suppress flow which is relevant in various fundamental and applied contexts of nanofluidics research [16, 35, 41, 42]. Experiments by Mattia *et al.* [43] reported EOF velocities exceeding those predicted by classical Poisson–Boltzmann (PB) models, suggesting missing physics in continuum descriptions. Mishra *et al.* demonstrated that incorporating dielectric saturation via the Langevin–Bikerman (LB) model improves electrostatic pressure predictions in steady-state PB formulations to match the experimental measurements. Building on this, Sinha *et al.* [44], Sin *et al.* [45] showed that including dipolar saturation effects can increase EOF mobility by up to 20% in nanochannels.

Srinivasula [46] systematically analyzed the steady state electroosmotic flow under fixed surface charge (FSC) as well as fixed surface potential (FSP) conditions relevant to various nanofluidic applications, including voltage-gated nanofluidic devices, demonstrating the surface condition importance in determining the significant dipolar solvent corrections to classical Poisson–Boltzmann based predictions. This distinguishes the use of functionalized surfaces of constant zeta potential from the gated voltage conditions of nanopores in applications. Di Muccio *et al.* [47] critically evaluated commonly used analytical approximations for electroosmotic flow in nanopores by benchmarking continuum predictions against atomistic simulations, showing that while continuum models accurately capture mean flow behavior, their validity hinges on incorporating field-dependent material responses under strong confinement. Blankenburg *et al.* [48] investigated nanoscale AC electroosmotic flow and demonstrated frequency–size scaling behavior that persists beyond the classical charge relaxation regime, highlighting the importance of transient electrohydrodynamic coupling rather than purely ionic time scales. Complementarily, Niu and Xie [49] analyzed electrohydrodynamics in ionic–surfactant-covered liquid films relevant to soft memristors, revealing strong nonlinear coupling between interfacial polarization, electric fields, and fluid stresses. Together, these works underscore that while continuum electrohydrodynamics remains a powerful framework at the nanoscale, predictive modeling of transient electroosmotic phenomena requires extensions that account for field-dependent interfacial and solvent physics.

This work is focused to address the gap in incorporating the dipolar solvent-dependent corrections to transient EDL and EOF evolutions by numerically implementing such a nonlinear formulation of a transient Poisson–Nernst–Planck–Stokes framework. This consistently incorporates the state-of-the-art dipolar solvent physics modeling through dielectric saturation and viscoelectric effects together.

## II. METHODOLOGY

The molecular and microscopic energetic contributions relevant to electrokinetic and electroviscous phenomena in aqueous and alike, dipolar-solvent nanofluidic systems are summarized in Israelachvili [50] together with their characteristic scalings and their individual treatments within the continuum frameworks. Short-range ion–ion electrostatic interactions, and to a lesser extent ion–dipole interactions, become significant at elevated ionic concentrations. While explicit treatments of ion–ion correlations have been reported for strong electrolytes [18], Kilic *et al.* [51] incorporated these effects implicitly as steric crowding in the electric double layer with a characteristic closest separation  $a$ . Combining this with a lattice-gas formulation, they formulated a modified Poisson–Nernst–Planck (MPNP) model[22]. Dipole–dipole interactions among solvent molecules, including

van der Waals contributions, cavity effects (modifies the local field acting on a dipole through the polarization of surrounding molecules by the external field), and reaction-field corrections (accounts for the self-interaction arising from response polarization of the surrounding medium by the dipole), are not resolved explicitly. Instead, their collective influence is absorbed into an effective solvent dipole moment chosen to reproduce bulk dielectric properties within continuum electrostatics [31, 52]. Hydrogen bonding, is known to strongly influence solvent structure and hydrodynamic response, from MD simulations capturing such inherent molecular complexity[53]. Within continuum modeling its net effect is instead represented phenomenologically through experimentally validated viscoelectric formulations [38–40].

Energetic contributions associated with the externally applied electric field, such as field self-energy and field–particle interactions, are included in the mean-field electrostatic free-energy relations [22]. In particular, the Langevin–Bikerman theory incorporates field–dipole coupling[50, 52] within a lattice-gas framework, yielding a field-dependent, spatially varying solvent permittivity under strong confinement [52]. While spatial variations in ion Born energies and dipole self-energies may become important in highly concentrated electrolytes[23], they are expected to be weak and partially compensated at the moderate concentrations considered here and are therefore not treated as separate energetic contributions. In nanoscale fluidics, the interfacial effects at the solid-electrolyte boundary often play a significant role in nanofluidics. While surface chemical reaction, pH regulation and Faradaic reaction flux conditions are used for specific electrode materials and operations, in this work, solid–electrolyte boundaries are modeled using Stern-layer conditions, which provide a generic representation of molecular adsorption and dielectric screening near insulating or weakly reactive surfaces [22, 52]. This classification clarifies a systematic selection of molecular and microscopic effects to be included for a tractable continuum description of nanofluidics for simulating weak to moderately concentrated aqueous-like electrolytes. Building on this continuum framework, the present formulation couples transient ionic transport, dipolar solvent polarization, and hydrodynamics within a unified continuum model.

### A. Electrostatics

Ionic dynamics are governed by the MPNP equations, capturing steric effects via the entropic terms in a lattice-gas formulation[22].

$$\epsilon_0 \epsilon_r \nabla^2 \psi = \rho_i \quad (1)$$

$$\frac{\partial n_{\pm}}{\partial t} = -\nabla \cdot J_{\pm} = D \left( \nabla^2 n_{\pm} \pm \beta e_0 \nabla \cdot (n_{\pm} \nabla \psi) + a^3 \nabla \cdot \left( \frac{n_{\pm} \nabla (n_{+} + n_{-})}{1 - n_{+} a^3 - n_{-} a^3} \right) \right) \quad (2)$$

Dipolar polarization responds instantaneously relative to ionic time scales and enters through a field-dependent, spatially varying permittivity obtained from an exponential fit to the Langevin–Bikerman (LB) model, addressed as the LB-fitted transient (LBFT) model, capturing dielectric saturation within the electric double layer. Dipolar solvent polarization is incorporated through a field-dependent, nonuniform permittivity  $\epsilon_r$  derived from LB theory[29], as described in the Appendix.

This would involve Strong adsorption, Permanent trapping or immobilization, Orientation locking, Dielectric discontinuities in the molecular spacing, and dipole-surface forces beyond those currently considered. Hence, the Stern layer is explicitly modeled with a lower permittivity. The Stern layer boundary condition is used with a molecular thickness, where the permittivity is approximated as a fraction of the bulk value.

$$V = \pm V_0 - \delta_s \epsilon \frac{\partial V}{\partial x}, \quad x = \pm L \quad (3)$$

Also, no species flux is used for insulating surfaces.

$$J_{\pm} = 0, \quad x = \pm L \quad (4)$$

### B. Hydrodynamics

In nanoscale systems, viscous momentum diffuses much faster than ionic charge relaxes. The characteristic viscous relaxation time is  $t_v = L^2/\nu$ , where  $L \sim 10\text{nm}$  is the length scale of the domain width and  $\nu \sim 10^{-6}\text{m}^2/\text{s}$  is the kinematic viscosity of water, giving  $t_v \sim 0.1\text{ns}$ . In contrast, the EDL charging time is  $\tau_{EDL} \sim \lambda_D L/D_{\pm}$ , where the Debye length  $\lambda_D \sim 1\text{nm}$  and  $D_{\pm} \sim 10^{-9}\text{m}^2/\text{s}$ , yielding  $\tau_{EDL} \sim 10\text{--}100\text{ns}$ . Since  $t_v \ll \tau_{EDL}$ , just like the molecular dipoles rotation, the velocity field rapidly equilibrates to any quasi-instantaneous distribution of charge on the EDL time scale. Therefore, the evolving ion profiles from the LBFT model can be consistently coupled to the steady Stokes equation to compute the time-dependent electroosmotic flow.

Electroosmotic flow (EOF) arises from the coupling between the electric double layer (EDL) and an externally applied tangential electric field. When a small lateral electric field  $E_l$  is applied along a charged surface, as shown in Figure 1(c), the net

ionic charge density  $\rho_i(x, t)$  present within the EDL exerts a body force on the surrounding fluid, generating the viscous shear-driven flow, a crucial phenomenon in electrokinetics and nanofluidics. In the low-Reynolds-number limit typical of nanoconfined flows, inertia is negligible, and the flow is governed by the steady Stokes equation. The electrohydrodynamic forcing enters the momentum balance as a body force term  $E_l \rho_i$ , yielding the one-dimensional form[54]:

$$\frac{d}{dx} \left( \eta_v \frac{du}{dx} \right) + E_l \rho_i = 0 \quad (5)$$

where  $\eta_v$  is the dynamic viscosity of the solvent, and  $v(x, t)$  is the velocity profile along the channel. with no slip condition on the surfaces.

$$u = 0, \quad x = \pm L \quad (6)$$

In line with experiments, the resulting flow is measured in terms of EOF mobility[54].

$$\mu_{eo} = \frac{1}{lE_l} \int_0^l u dx \quad (7)$$

This integral form naturally incorporates both near-wall dynamics and bulk transport contributions, making it particularly suitable for comparing different continuum models, such as those based on PNP, MPNP, or LBFT model.

The hydrodynamic influence of solvent molecular network restructuring on momentum transport is included phenomenologically through a field-dependent viscosity using the viscoelectric effect[38].

$$\eta_v = \eta_0(1 + f_v E^2) \quad (8)$$

with the value of  $f_v = 1.02 \times 10^{-15} \text{m}^2/\text{V}^2$ . Here,  $\eta_0$  is the zero-field viscosity and  $f_v$  is the coefficient characterizing the strength of viscoelectric effects. Together, these equations enable a numerically tractable, consistent description of transient electric double layer formation and electroosmotic flow in nanoscale systems.

Electrohydrodynamic (EHD) forces describe the momentum transfer from electric fields to a fluid due to the presence of mobile and bound charges. At the continuum scale, this coupling is encapsulated in the Maxwell stress formulation, which has long served as a cornerstone in electrohydrodynamic theory. In nanofluidic systems, where field gradients are strong and dielectric properties vary at molecular scales, resolving these forces becomes essential to accurately modeling pressure development and stress-driven instabilities near surfaces. Following the classical electrohydrodynamics framework by Saville [55], the volumetric EHD force density is given as,  $\mathbf{\Pi}_e = \rho_i \mathbf{E} + \mathbf{P} \cdot \nabla \mathbf{E}$ . The first term represents the direct Coulombic force on ions. The second term, with polarization density vector  $\mathbf{P}$ , accounts for dielectrophoretic forces acting on aligned dipolar solvent molecules in a nonuniform electric field. Such interactions are responsible for dielectric body forces, even in the absence of free charge. Unlike many classical electrokinetic studies where permittivity is treated as uniform, the present model allows a spatially nonuniform  $\mathbf{P}$  (inline with  $\epsilon_r$ ), capturing solvent reorientation under applied fields.

### C. Problem setup

For solvent molecular dipole moment,  $p_0$ , we can write  $p_0 E \beta = \hat{p}_0 \tilde{E}$  in terms of the electric field normalized with the nominal field in the fully developed EDL  $\tilde{E} = E/E_D = E \lambda_D / \Delta V$ . Hence,  $\hat{p}_0 = p_0 E_0 \beta / \epsilon$ .

$$\hat{c}_i = \frac{c_i}{2c_0}, \quad \hat{\psi} = \frac{\Psi}{1/(ze\beta)}, \quad \hat{x} = \frac{x}{L}, \quad \hat{t} = \frac{t}{\tau_v} \quad (9)$$

Where the  $\tau_v = \frac{\lambda_{Dv} L}{D}$  is the time scale of ion dynamics of EDL formation in vacuum, corresponding to Debye length  $\lambda_{Dv} = \sqrt{\frac{\epsilon_0}{2c_0 z^2 e^2 \beta}}$ . Some useful dimensionless parameters can be defined as follows.

$$\epsilon = \frac{\lambda_{Dv}}{L}, \quad \delta_s = \frac{\lambda_s}{\lambda_{Dv}}, \quad \hat{c}_0 = \frac{2c_0}{c_L}, \quad v = \frac{V}{1/(ze\beta)}, \quad \hat{p}_0 = \frac{p_0}{zeL} \quad (10)$$

Also,  $\hat{p}_i = \rho_i / 2c_0 e$ .

A velocity scale  $u_{HS} = \epsilon_0 \epsilon_r e E_l / (e \beta \eta_{0v})$ , more popularly identified as the classical Helmholtz–Smoluchowski scale for the electroosmotic velocity, corresponds to the velocity generated by a surface potential of order the thermal voltage,  $\zeta \sim 1/(e\beta)$

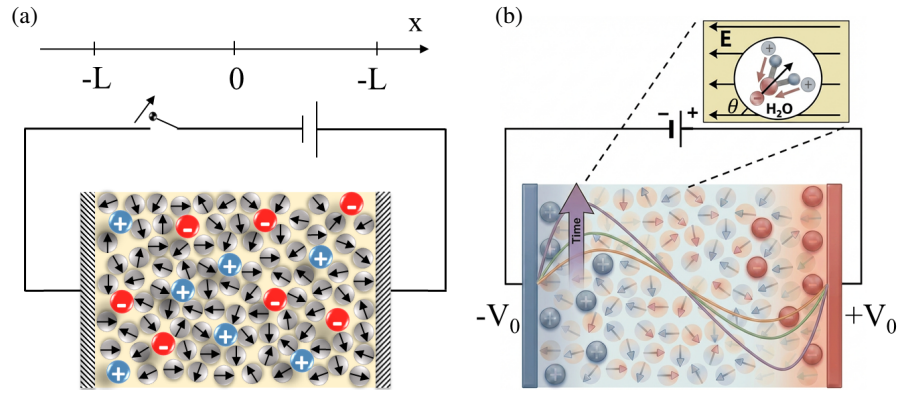


FIG. 1. Illustration of the electrolytic cell (a) before and (b) after applying external voltage ( $2V_0$ ). (c) Transient growth of EOF velocity profile ( $u_{eo}$ ) under a small lateral electric field ( $E_l$ ), with range of dipolar solvent corrections highlighted.

under a weak lateral field  $E_l$ . This normalization provides a meaningful reference scale to compare EOF magnitudes across models that incorporate steric, dipolar, or viscoelectric effects. Consistent with the above scaling, the dimensionless electroosmotic mobility is  $\hat{\mu}_{eo} = \int_0^1 \hat{u} d\hat{x}$ .

The charge dynamics in an electrolyte in a block between two closely placed large parallel plate electrodes was studied using PNP and MPNP models by [56] and [22], respectively. Consideration of the steric influence in the later reduces the crowding of the counter-ions in the EDL, although the time and length scales remain nearly the same. The influence of the dipolar solvent molecules in such a setup with the same boundary and initial conditions is analyzed below, using the above dPNP model.

Consider a univalent salt of concentration  $c_0$  dissolved in water in the domain shown in the figure. The separation between the plates is  $2L$  and a step voltage of amplitude  $2V$  is suddenly applied at time  $t = 0$ . An insulating surface is assumed on the electrodes with no Faradaic reactions or charge injection. Stern layer is considered with a fixed relative permittivity and no charge density to represent the interaction between the electrode and dipolar solvent molecules stuck to the surface. Thickness of the Stern layer is  $\lambda_s$  and relative permittivity is  $\epsilon_{rs}$ . Estimating the relative permittivity (dielectric constant) of the Stern layer in an electrolytic cell is a nuanced task, as this parameter is influenced by several interrelated factors at the electrode–electrolyte interface. It depends on factors such as solvent molecules orientation and ionic charge in the adsorbed layer and strength of the electric field or surface charge density. In this study, the surface voltage or charge is kept fixed, and the Stern layer permittivity is assumed to be 70% of the bulk value of the electrolyte[46]. This is to define a controllable contribution of the surface chemistry while analyzing the solvent-based physics in the study.

Electrolyte species are separated from the electrode surfaces by the Stern layers in  $\hat{x} \in [-1, -(1 - \epsilon\delta_s)]$  and  $\hat{x} \in [(1 - \epsilon\delta_s), 1]$ . Hence, the Stern layers of a fixed relative permittivity and no charge are sandwiched between the electrode boundaries and the electric double layers. The Laplace equation is solved with the corresponding fixed relative permittivity without ionic species.

$$\epsilon_r = \begin{cases} 1, & -(1 - \epsilon\delta_s) \leq \hat{x} \leq (1 - \epsilon\delta_s) \\ \epsilon_{rs}, & \hat{x} < -(1 - \epsilon\delta_s) \text{ or } \hat{x} > (1 - \epsilon\delta_s). \end{cases} \quad (11)$$

with boundary condition

$$\psi = \pm V_0, \quad x = \pm l \quad (12)$$

The electric field is applied suddenly at time  $t = 0$ , hence, the initial condition for the transient study is similar to that used by [56].

$$\hat{\psi}(\hat{x}, t) = vx, \quad \text{at } t = 0, \forall x \in [-1, 1]. \quad (13)$$

The ionic species are uniformly distributed before the electric field is applied and their perturbation begins at  $t = 0$ . Hence,

$$\hat{c}_{\pm}(\hat{x}, t) = 0.5, \quad \text{at } t = 0, \forall x. \quad (14)$$

EDL charging is examined in a symmetric monovalent electrolyte of equal diffusivity confined between two large, planar electrodes under a step voltage  $2V$  with separation  $2L$ , applied at  $t = 0$ , following Kilic *et al.* [22], as shown in Figures 1(a,b). The electrolyte, with bulk ion concentration  $c_0$ , is dissolved in water of molecular density  $c_{0s} = 55000$  mM, modeled using an effective dipole moment higher than isolated molecules  $p_0 \approx 4.7\text{--}5$  D [29, 31]. Electrodes are modeled as ideally polarizable (no Faradaic reactions) Stern layers of thickness  $\lambda_s = a/2$  and permittivity approximated as  $\epsilon_{rs} = 0.7\epsilon_{r0}$  accounts for interfacial solvent immobilization. Where, under weak-field conditions, this yields a uniform bulk permittivity  $\epsilon_{r0} = 1 + c_{0s}p_0^2\beta/(3\epsilon_0)$ .

The scaling based on the Helmholtz–Smoluchowski’s estimate,  $\mu_{HS} = \epsilon_0 \epsilon_{r0} k_B T / (e \eta_v)$  is of the order  $1.5 - 2 \times 10^{-8} \text{ m}^2 / (\text{V}\cdot\text{s})$  for the nanoscale systems of interest in this work. To facilitate comparison of electrohydrodynamic (EHD) responses across models, the dimensionless force density ( $\tilde{\Pi}_e$ ) can be further normalized using the standard Maxwell stress scale,  $\Pi_0 = \epsilon_0 \epsilon_{r0} E_{0_{edl}}^2 / \lambda_D$ . Here  $E_{0_{edl}} = 1 / (e \beta \lambda_D)$  is the characteristic electric field within the electric double layer (EDL). This scaling is motivated by the fact that EHD forces are most significant near the charged surfaces, where the electric fields are mostly confined with steep gradients, while they diminish rapidly in the bulk where electrostatic screening suppresses field variations. This gives,

$$\tilde{\Pi}_e = \epsilon \left( \hat{\rho}_i \hat{E} - \hat{\rho}_0 \hat{c}_s \mathcal{L}(\hat{\rho}_0 \hat{E}) \frac{\partial \hat{E}}{\partial \hat{x}} \right), \quad \mathcal{L}(\hat{\rho}_0 \hat{E}) = \coth(\hat{\rho}_0 \hat{E}) - \frac{1}{\hat{\rho}_0 \hat{E}}. \quad (15)$$

A dimensionless number can be defined to quantify the dipolar solvent effect as  $\alpha_2 = p_0 E \beta$ . (Notation  $\alpha_2$  is used consistent with the *joint PRL submission*.) For  $\alpha_2 \ll 1$ ,  $\mathcal{F} \approx \alpha_2 / 3$  and  $\mathcal{H} \approx n_{0w} (1 + (2n_0 / n_{0w}) \cosh(\hat{V}_0 \hat{\psi}))$ , for  $\hat{\psi} = \psi / V_0$ . Recovers MPNP for small dipolar solvent effect ( $\alpha_2 \ll 1$ ) with small electric potential perturbation ( $\hat{V}_0 \ll 1$ ) or low ionic concentration ( $\hat{c}_0 \ll 1$ ). Hence, the relative permittivity approximates to,  $\epsilon_r \approx \epsilon_{r0} = 1 + n_s p_0^2 \beta / 3 \epsilon_0$ . Thus, the LBFT model results in MPNP model of Kilic *et al.* [22].

#### D. Numerical implementation

The numerical procedure is developed to cater both LBFT-S from this work and for solving the dPNP-S model from the *joint PRL submission* as well. The above equations are solved in the electrolyte domain  $\hat{x} \in [-(1 - \epsilon \delta_s), (1 - \epsilon \delta_s)]$ , while the Laplace equation is solved in the Stern layers. Boundaries at  $\hat{x} = \pm 1$  assume applied potential  $\hat{\psi} = \pm \hat{V}_0$ , while no ionic flux is prescribed at the Stern layer boundaries at  $\hat{x} = \pm(1 - \epsilon \delta_s)$  maintaining electric potential continuity. The initial state assumes uniform ion concentration  $\hat{c}_{\pm} = 0.5$  and linear potential profile  $\hat{\psi} = \hat{V}_0 \hat{x}$ . Solving the time-dependent LBFT equations under a sudden voltage step is implemented in the 1D model in COMSOL Multiphysics v6.2, leveraging its state-of-the-art finite element method (FEM) framework. The Nernst–Planck equations are discretized using quadratic (P2) elements, while the Poisson equation uses cubic (P3) elements to capture sharp spatial variations in the electrostatic potential and polarization fields. A highly refined nonuniform mesh is employed: the near-wall region up to  $\delta_s + 10\epsilon$  is discretized with 1500 equally spaced elements, and the remaining bulk domain with elements of size  $\epsilon / 25$ , ensuring grid-independent results.

Time integration is performed using the generalized- $\alpha$  method, a second-order implicit scheme designed for stiff, transient PDEs. The maximum time step is restricted to  $10^{-3}$ , with a relative solver tolerance of 2%. To maintain stability without sacrificing accuracy during fast charging phases, the high-frequency dissipation factor in the  $\alpha$ -method is tuned between 0.5–0.75, selectively damping numerical noise without suppressing true dynamics.

At each time step, the nonlinear system is solved using Newton’s method, with up to 8 iterations and an adaptive line search strategy. We activate the “Highly nonlinear Newton” setting to enhance robustness via step-size damping and automatic back-tracking. In particular, a recovery damping factor of 0.2–0.75 is employed when residuals temporarily increase, allowing safe step-size reduction and recovery from divergence. A minimum damping factor of 0.001 ensures conservative updates when strong nonlinearity is encountered. If convergence stalls, the Newton step size is reduced by a factor of 10 before reattempting. The resulting linearized system is solved at each Newton step using the MUMPS (Multifrontal Massively Parallel Sparse) direct solver, which performs robust LU factorization optimized for large, sparse, and ill-conditioned matrices.

The strongly nonlinear coupling in the dPNP equations involving steep gradients of electric field and Langevin functions, especially near charged interfaces under a sudden voltage step, poses significant numerical challenges. The 1D model is solved in COMSOL v6.2 using finite elements: quadratic elements for the Nernst–Planck equations and cubic elements for Poisson’s equation. A refined mesh of 1500 uniform elements is used near the walls (up to a distance  $\delta_s + 10\epsilon$ ), with the remaining bulk discretized at  $\epsilon / 25$  resolution. Time integration employs adaptive time stepping with the implicit second-order generalized- $\alpha$  method with a maximum step size limited to  $10^{-3}$  and a relative tolerance of 0.02. High-frequency damping (factor 0.5–0.75) is tuned to stabilize stiff transients without degrading accuracy. Newton’s method is used at each time step with up to 8 iterations after preconditioning, with conservative damping, and a recovery damping factor of 0.2–0.75 for robust convergence. The linearized systems are solved using the MUMPS direct solver with full LU factorization and reordering to ensure accuracy and stability.

Simulations at five combinations of parameters relevant for modern voltage-gated applications such as nanofluidic logic and biosensing, listed in table I, are conducted using the three models- LBFT, MPNP, and PNP. These cases of parameters and the anticipated time scales of the EDL dynamics and transient EOF dynamics ( $\tau_D \sim 10 \text{ ns}$ ) are relevant to voltage-gated applications in nanofluidic logic circuits [4, 5] and DNA sequencing [9] applications. Case I indicates a domain of length 25 nm, with molecular dipole moment of the solvent close to that of the effective dipole moment of water[31]. Case II demonstrates a reduced channel width ( $L = 10 \text{ nm}$ ), case III has a slightly weaker dipole moment yet relevant to aqueous electrolytes ( $p_0 = 4.75 \text{ D}$ ), case IV has a thick EDL due to lower ion concentration ( $c_0 = 0.1 \text{ mM}$ ), and case V has a lower applied voltage ( $V_0 = 20 \text{ mV}$ ). Comparisons of results from these cases serve for isolating different parameteric influences.

TABLE I. Simulation parameters for the four representative cases considered in this study, selected to reflect relevant application conditions. The temperature is fixed at 290 K for all cases.

Case	$L$ (nm)	$c_0$ (mM)	$p_0$ (D)	$V_0$ (V)	$\varepsilon$	$\alpha_2$	$\hat{\varepsilon}_0$	$\hat{V}_0$
I	25	100	4.95	0.25	0.039	0.0041	3.6	10
II	10	100	4.95	0.10	0.099	0.0103	3.6	4
III	10	100	4.75	0.10	0.095	0.0099	3.6	4
IV	10	0.1	4.95	0.10	3.144	0.0103	0.0036	4
V	10	100	4.95	0.01	0.099	0.0103	3.6	0.4

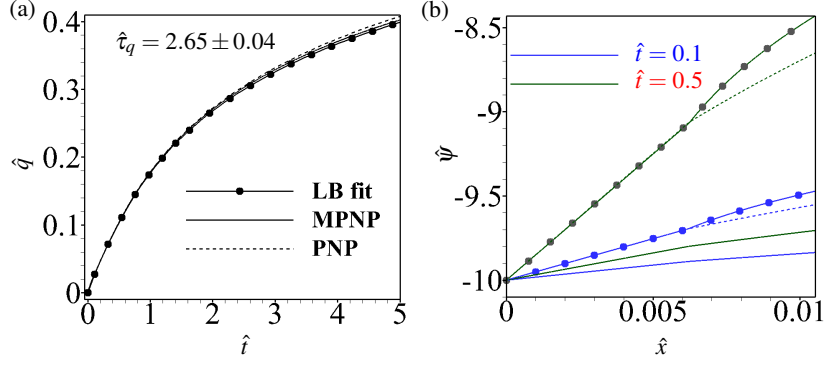


FIG. 2. (a) Temporal evolution of the total EDL charge predicted by the different models for Case I. (b) Spatial variation of the electric potential as a function of distance from the electrode surface for Case I, shown at two representative times. The region  $\hat{x} < 0.006$  corresponds to the Stern layer. (Color online.)

### III. RESULTS AND ANALYSIS

#### A. Transient EDL Dynamics

The nonuniform permittivity arising from dipolar solvent response modifies the charging dynamics of the electric double layer (EDL). The total diffuse charge density accumulated near the surface, beyond the Stern layer, is quantified as

$$\hat{q} = \int_{-1+\varepsilon\delta_s}^{-1+10\varepsilon} \hat{\rho} d\hat{x}.$$

For Case I, the value of  $\hat{q}$  predicted by the LBFT model closely follows those obtained from the MPNP and classical PNP formulations, as shown in Fig. 2(a). Any noticeable deviations emerge only at later times, where the LBFT estimate is slightly higher than the MPNP prediction. The exponentially fitted charging time scales ( $\hat{\tau}_q$ ) remain nearly identical across all models, consistent with steric-modified PNP behavior reported by Kilic *et al.* [22]. These results indicate that dipolar solvent corrections primarily affect the magnitude of the accumulated charge while leaving the global charging time constant essentially unchanged.

Figure 2(b) shows the electric potential distribution in the vicinity of the electrode, including the Stern layer, at two representative instants during the transient evolution of the EDL for Case I. As the space charge develops, the normal electric field at the Stern–diffuse interface adjusts dynamically, resulting in a time-dependent redistribution of the voltage drop across the Stern layer. The electric potential evaluated at the Stern–electrolyte boundary ( $\hat{x} = 0.006$ ) predicted by the LBFT model differs systematically from the MPNP and PNP results due to the field-dependent dielectric response associated with dipolar solvent effects. This behavior is consistent with previously reported steady-state analyses [46] and is shown here to persist throughout the transient regime.

The instantaneous charge structure is further examined in Fig. 3 at an intermediate time  $\hat{t} = 2.7$  for Cases I and IV, both near and away from the Stern boundary. Owing to antisymmetry about the channel mid-plane ( $\hat{x} = 0$ ), only one half of the domain is shown. The charge density near the negatively charged electrode is plotted as a function of the distance  $\hat{d}$  measured from the Stern–EDL interface located at  $\hat{x} = -1 + \varepsilon\delta_s$ , defined as  $\hat{d} = 1 + \hat{x} - \varepsilon\delta_s$ . In the near-surface region [Fig. 3(a)], the LBFT model predicts a higher ionic charge density for Case I. This increase arises from reduced dielectric screening under strong electric fields, which enhances charge accumulation close to the interface. In contrast, Case IV corresponds to a dilute electrolyte with a comparatively thick EDL, where the Debye length exceeds the characteristic domain scale due to the smaller value of  $\alpha_2$

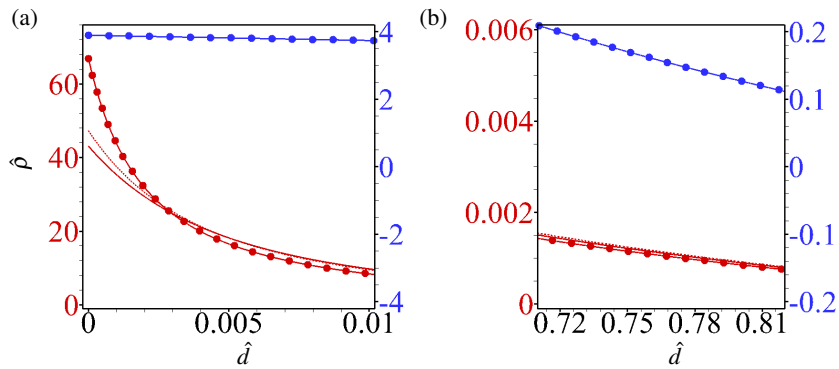


FIG. 3. (a, b) Distributions of charge density from different models, at  $\hat{t} = 2.7$  for case I (red) & IV (blue) near and away from the surface, respectively. See Figure 2(a) for the legend. (Color online.)

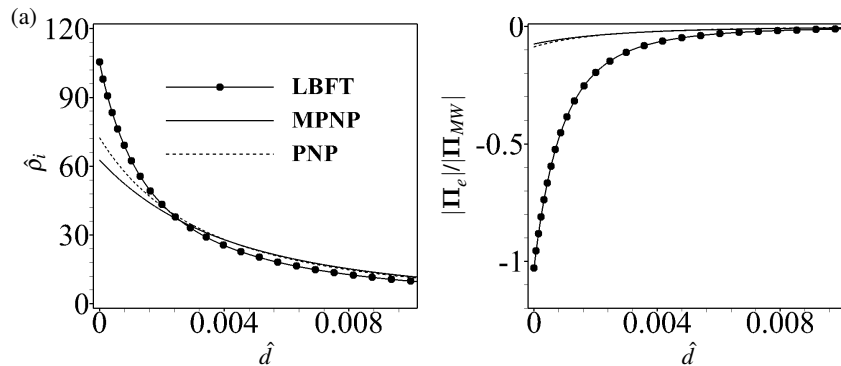


FIG. 4. (a) The scaled space charge density and (b) normalized EHD force density profiles at  $\hat{t} = 5$  for case I. (Color online.)

(representative of typical aqueous electrolytes). Under these conditions, the LBFT predictions become nearly indistinguishable from those of the MPNP and PNP models.

Farther from the surface [Fig. 3(b)], the electric field is largely screened by the diffuse layer. To maintain global charge balance, the LBFT model yields a slightly lower charge density in the outer region relative to the MPNP and PNP predictions. Although these spatial redistributions are subtle, the present results indicate their significant influence on the transient behavior of the system.

## B. Transient Electrohydrodynamic Response

The space-charge distribution and the resulting electrohydrodynamic (EHD) force density are shown in Fig. 4 at  $\hat{t} = 5.0$  for Case I. The dPNP model predicts a substantially enhanced near-surface Maxwell force density, reaching values up to an order of magnitude larger than those obtained from the classical PNP and MPNP formulations. This amplification is more pronounced than the corresponding increase in ionic charge density and arises primarily from the dipolar solvent contribution under dielectric saturation, which strengthens the local electric field gradients adjacent to the electrode.

Because the hydrodynamic response is highly sensitive to the spatial distribution of interfacial body forces, these amplified near-wall EHD stresses exert a disproportionate influence on the transient flow dynamics. The results therefore indicate that a dynamically coupled dipolar solvent response, rather than a purely ionic description of the EDL, is necessary for quantitatively accurate modeling of nanoscale electrohydrodynamics.

### 1. Dielectric Saturation Effect on Transient Electroosmotic Flow

The velocity profiles predicted by the different electrostatic models, excluding the viscoelectric correction ( $f_v = 0$ ) in the Stokes equation, are shown in Fig. 5(a) at two representative instants during the spatiotemporal evolution of electroosmotic flow (EOF). Under the no-slip boundary condition at the wall, the modest reduction in charge density away from the surface

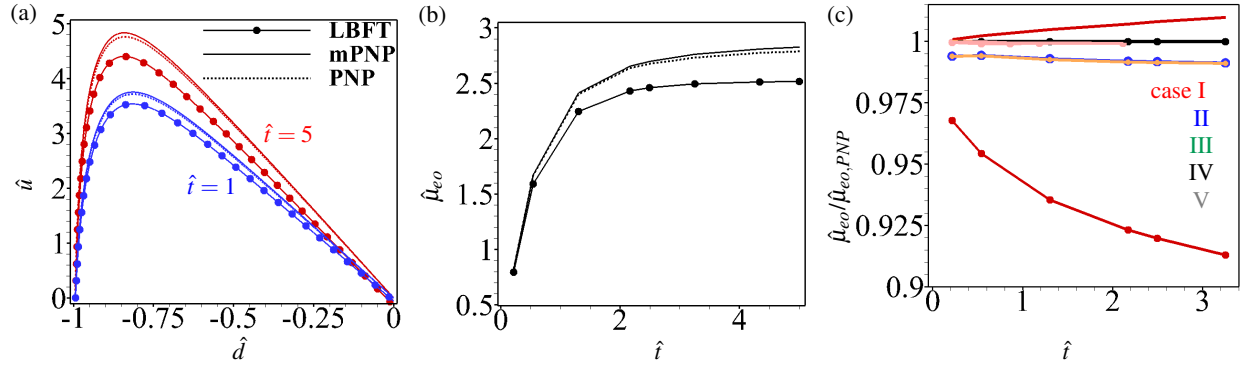


FIG. 5. Transient EOF with dielectric saturation and no viscoelectric effect of LBFT model. (a) Spatio-temporal profiles of EOF velocity from different models for case I and corresponding (b) EOF mobility evolutions with time. (c) Evolution of correction factors for EOF mobility for LBFT, MPNP models relative to PNP for the different cases shown in different colors. (Color online.)

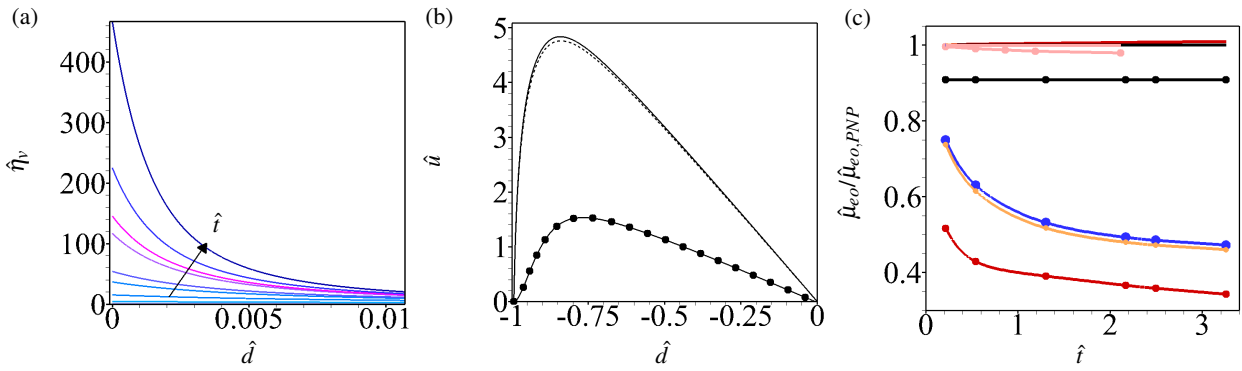


FIG. 6. Transient EOF with dielectric saturation and viscoelectric effects of LBFT model compared to traditional PNP/MPNP- Stokes models. (a) Spatio-temporal evolution of viscosity in LBFT model, (b) velocity profile estimates from different models at  $\hat{t} = 5$  for case I. (c) EOF mobility correction factors of LBFT with viscoelectric effects compared to PNP model, at  $\hat{t} = 5$ . (Legends same as figure 5.) (Color online.)

outweighs the pronounced near-surface increase observed in Fig. 3. Consequently, the LBFT model predicts a slightly lower bulk EOF velocity compared with the classical PNP and modified PNP (MPNP) formulations. This trend is consistent with the steady-state comparison reported in Srinivasula [46, Fig. 4], where the Langevin–Bikerman model yields a reduced EOF velocity relative to the Poisson–Boltzmann limit, particularly in the weak dipolar regime ( $\hat{p}_0 \ll 1$ ). The influence of dielectric saturation on the transient velocity profiles becomes progressively more pronounced as the system evolves toward steady state.

The corresponding transient evolution of the normalized electroosmotic mobility,  $\hat{\mu}_{eo}$ , is shown in Fig. 5(b). All models exhibit a monotonic increase toward their respective steady-state values; however, the LBFT prediction consistently remains lower, reflecting the cumulative influence of dielectric saturation on the effective electrohydrodynamic driving force within the diffuse layer.

Figure 5(c) presents the temporal variation of the mobility ratios predicted by the LBFT and MPNP models relative to the classical PNP formulation across parametric Cases I–V. The MPNP correction factors remain close to unity for all cases, indicating that ion steric effects introduce only minor quantitative changes to the EOF mobility under the present conditions. In contrast, the dipolar corrections incorporated in the LBFT model are more pronounced, particularly for Case IV, which corresponds to a comparatively thick EDL. In this regime, dipolar modifications to the diffuse charge extend farther into the bulk, leading to a larger reduction in electroosmotic mobility as the system approaches steady state, although the dielectric saturation itself is weaker due to the lower near-surface charge density and electric field.

## 2. Viscoelectric Effect on Transient Electroosmotic Flow

Figure 6 presents the electroosmotic flow (EOF) predicted by the LBFT model with viscoelectric effects included for an aqueous-like dipolar solvent, using the coefficient  $f_v = 1.02 \text{ m}^2/\text{V}^2$  [38, 40, 41]. The spatiotemporal evolution of the viscosity

field is shown in Fig. 6(a). A pronounced viscosity enhancement develops within the electric double layer (EDL), where the electric field is strongest and dipolar alignment is most significant during the transient EDL evolution. Outside the EDL, the viscosity rapidly relaxes toward its bulk value as the electric field weakens, indicating that the viscoelectric correction remains strongly localized near the interface.

The corresponding EOF velocity profiles at  $\hat{t} = 5$  predicted by the different electrostatic models are shown in Fig. 6(b). The increased near-wall viscosity in the LBFT formulation substantially reduces the peak velocity while preserving the qualitative ordering among the models. In addition to lowering the overall flow magnitude, the viscoelectric contribution modifies the transient electroosmotic response through the combined action of dielectric saturation and field-dependent viscous resistance, both arising from the dipolar nature of the solvent.

This combined influence is further illustrated in Fig. 6(c), which shows the temporal evolution of the electroosmotic mobility correction ratios. Cases I and IV, characterized by comparatively weaker nominal electric fields, exhibit modest corrections, whereas the remaining cases display increasingly pronounced deviations that grow with time as the system approaches steady state.

Overall, these results demonstrate that the coupled dielectric and viscoelectric responses of a dipolar solvent can significantly modify transient nanoscale electroosmotic transport. Neglecting either mechanism may therefore lead to systematic overprediction of electroosmotic velocities in strongly driven nanofluidic regimes.

#### IV. DISCUSSION

Dipolar solvent corrections applied solely to the relative permittivity produce a noticeable deviation of the LBFT model from the mPNP formulation primarily for Case I. However, when both permittivity and viscosity corrections are incorporated within the LBFT–Stokes framework, departures from the corresponding mPNP–Stokes model arise for Cases I–III. In contrast, when the dimensionless parameter  $\alpha_2 \ll 1$  and either the bulk concentration  $\hat{c}_0$  or the applied potential  $\hat{V}_0$  is small, as in Cases IV and V, the predictions of the LBFT model become nearly indistinguishable from those of the traditional mPNP formulation. Indicating the criteria for a strong dipolar solvent effect. All-in-all, compared with the constant-property PNP model, the LBFT formulation systematically predicts reduced electroosmotic mobility. The steady-state mobility in Case I is lower by up to 10–20%, while the combined dipolar-solvent and viscoelectric effects can suppress the mobility by up to 50–60% under strong electric-field conditions.

Direct comparisons with previously reported transient electrokinetic simulations or experiments remain limited, as most existing nanoscale studies have focused on steady-state formulations of dipolar continuum models. Nevertheless, the present framework provides a basis for analyzing time-dependent electrohydrodynamic processes in nanoscale systems. Although the present study considers the transient response following a step application of electric potential across a nanoconfined electrolyte, the model can be extended naturally to time dependent forcing, such as AC potentials applied across nanopores or nanochannels. In such systems, the advective contribution to ionic transport could be, typically, weaker; however, including this effect would enable a fully coupled electrohydrodynamic description and may be pursued in future work.

Extension of the present framework to higher-dimensional geometries may reveal additional consequences of dipolar solvent response. In particular, spatial variations of permittivity and charge density can generate tangential Maxwell stresses that drive secondary electrohydrodynamic phenomena, including electroviscous effects arising from coupled ion and fluid transport. Such mechanisms may become especially relevant in nanoconfined flows where strong electric fields coexist with geometric confinement.

Transient EDL dynamics may also play a role in emerging nanofluidic technologies such as nanopore biosensing and DNA sequencing. During molecular translocation through nanopores, the local ionic environment evolves dynamically in response to both rapid molecular motion and time-dependent electric forcing. Because the characteristic time scale for EDL relaxation can be comparable to molecular transit times, nonequilibrium charge structures may persist and influence ionic current signals. A physically grounded transient EDL framework therefore has the potential to complement data-driven approaches currently used in nanopore signal analysis by providing mechanistic insight into the electrostatic environment surrounding translocating biomolecules [57, 58].

Finally, the LBFT formulation provides a computationally efficient approximation for incorporating dipolar solvent physics into continuum electrokinetic models. In the present implementation, nonuniform but time-invariant permittivity and viscosity fields are employed, consistent with current continuum modeling practices. A more complete formulation with fully time-dependent dipolar coupling, referred to as the dipolar PNPS (dPNPS) model, is developed separately in *joint PRL submission*. Although the dPNPS model provides a more rigorous description of solvent polarization dynamics, it is computationally more demanding. For a representative simulation on a workstation with a 4 GHz processor and 16 GB RAM, the LBFT–Stokes model requires approximately 15 minutes of computation time, whereas the dPNPS model requires roughly 100 minutes. The LBFT approach therefore offers a practical compromise between physical fidelity and computational efficiency, making it attractive for engineering analyses of transient nanofluidic systems.

## V. CONCLUSIONS

This work extends Langevin–Bikerman-type solvent modeling to transient nanoscale electrohydrodynamics. The classical one-dimensional electrolytic cell problem, widely used to study time-dependent PNP formulations for EDL charging with Stern layers and steric effects [22, 56], is revisited here with the co-evolution of ionic distributions, field-dependent permittivity, and hydrodynamic response under the Stokes flow and weak ionic advection limits. The results show that dielectric saturation alone can reduce electroosmotic mobility by up to 10% relative to standard PNP predictions, while its combined action with the viscoelectric effect leads to reductions as large as 70%. Although the dominant correction arises from viscoelectricity, the transient evolution of the response depends on the coupled action of both mechanisms. Within the familiar PNP–Stokes framework, the proposed LB-fitted transient (LBFT) model provides a tractable continuum approach for incorporating dipolar solvent physics into nanoscale electrohydrodynamic simulations, enabling classical fluid-mechanical analysis to be extended from microfluidic regimes toward emerging ultrafast nanofluidic systems.

## DECLARATIONS

No data were created or used in this study. This research received no specific grant from any funding agency. The author declares no competing interests.

## Appendix A: Appendixes

### 1. Steadystate modeling with dipolar solvent

Langevin-Bikerman (LB) model [52] is a steady state model that incorporates dipolar solvent effects via nonuniform permittivity given by,

$$\varepsilon_r = 1 + n_{0w}n_s \frac{p_0}{\varepsilon_0} \frac{\mathcal{F}}{E\mathcal{H}} \quad (\text{A1})$$

$$\mathcal{F} = \left( \coth(p_0E\beta) - \frac{1}{p_0E\beta} \right) \frac{\sinh(p_0E\beta)}{p_0E\beta} \quad (\text{A2})$$

$$\mathcal{H} = 2n_0 \cosh(e_0\psi\beta) + n_{0w} \frac{\sinh(p_0E\beta)}{p_0E\beta}, \quad (\text{A3})$$

into PB model as

$$\nabla \cdot (\varepsilon_0 \varepsilon_r \nabla \psi) = -\rho_i^{LB} \quad (\text{A4})$$

$$\rho_i^{LB} = -2e_0 n_0 n_s \frac{\sinh(e_0\beta\psi)}{\mathcal{H}}. \quad (\text{A5})$$

Here  $n_0$  denotes the bulk ionic concentration,  $n_{0w}$  the bulk solvent concentration,  $p_0$  the effective solvent dipole moment, and  $\beta = (k_B T)^{-1}$ . Following classical electrochemical cell models, we consider one half of a symmetric electrolyte domain bounded by a Stern layer adjacent to the electrode. The LB equations are solved in the diffuse layer,  $-(1 - \varepsilon\delta_s) \leq \hat{x} \leq 0$ , while a Laplace equation governs the Stern layer,  $-1 \leq \hat{x} < -(1 - \varepsilon\delta_s)$ . A fixed applied potential  $\hat{\psi} = -v$  is prescribed at the electrode surface, and for  $\varepsilon \ll 1$  the bulk boundary is taken to be electrically neutral,  $\nabla \hat{\psi} = 0$ , ensuring an unperturbed far-field electrolyte.

Spatially nonuniform permittivity of case I obtained from the LB model is shown in Figure 7. As counterions move to the surface and increase the electric field and its gradient, solvent concentration decreases, and the polarization density decreases[52]. This results in lower permittivity, as seen in the figure, estimated by the LB model [see 52, eq. 36–38]. An exponential profile fitted to the LB solution is also shown here, which is used in the LBFT model for this parametric case.

- 
- [1] W. Wang, Y. Ma, and Y. Liang, Field-effect nanofluidic memristor, *Physics of Fluids* **37** (2025).
  - [2] D. V. Melnikov, N. R. Barker, and M. E. Gracheva, Ionic current blockade in a nanopore due to an ellipsoidal particle, *Physical Review E* **110**, 034403 (2024).
  - [3] R. Dolatshahi, M. Khatibi, and S. N. Ashrafizadeh, Salinity gradient energy harvesting via tuned ionic nanotransistor geometries, *Physics of Fluids* **37** (2025).
  - [4] W. Guan, R. Fan, and M. A. Reed, Field-effect reconfigurable nanofluidic ionic diodes, *Nature communications* **2**, 506 (2011).
  - [5] P. Robin, T. Emmerich, A. Ismail, A. Niguès, Y. You, G.-H. Nam, A. Keerthi, A. Siria, A. Geim, B. Radha, *et al.*, Long-term memory and synapse-like dynamics in two-dimensional nanofluidic channels, *Science* **379**, 161 (2023).

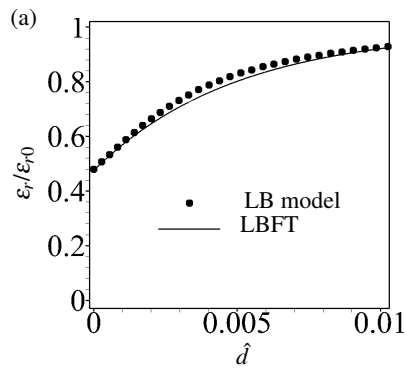


FIG. 7. Spatial profile of permittivity from LBFT and its mathematical fitted function for case I.

- [6] W. Liu, T. Mei, Z. Cao, C. Li, Y. Wu, L. Wang, G. Xu, Y. Chen, Y. Zhou, S. Wang, *et al.*, Bioinspired carbon nanotube-based nanofluidic ionic transistor with ultrahigh switching capabilities for logic circuits, *Science Advances* **10**, eadj7867 (2024).
- [7] T. Emmerich, Y. Teng, N. Ronceray, E. Lopriore, R. Chiesa, A. Chervov, V. Artemov, M. Di Ventra, A. Kis, and A. Radenovic, Nanofluidic logic with mechano-ionic memristive switches, *Nature Electronics* **7**, 271 (2024).
- [8] Y. He, M. Tsutsui, C. Fan, M. Taniguchi, and T. Kawai, Gate manipulation of dna capture into nanopores, *ACS nano* **5**, 8391 (2011).
- [9] Y. He, M. Tsutsui, C. Fan, M. Taniguchi, and T. Kawai, Controlling dna translocation through gate modulation of nanopore wall surface charges, *ACS nano* **5**, 5509 (2011).
- [10] J. Wei, H. Hong, X. Wang, X. Lei, M. Ye, and Z. Liu, Nanopore-based sensors for dna sequencing: a review, *Nanoscale* **16**, 18732 (2024).
- [11] H. Tian, M. A. Alkhadra, and M. Z. Bazant, Theory of shock electro dialysis i: Water dissociation and electrosmotic vortices, *Journal of Colloid and Interface Science* **589**, 605 (2021).
- [12] J. De Valenca, M. Jogi, R. M. Wagterveld, E. Karatay, J. A. Wood, and R. G. Lammertink, Confined electroconvective vortices at structured ion exchange membranes, *Langmuir* **34**, 2455 (2018).
- [13] J. Choi, M. Cho, J. Shin, R. Kwak, and B. Kim, Electroconvective instability at the surface of one-dimensionally patterned ion exchange membranes, *Journal of Membrane Science* **691**, 122256 (2024).
- [14] A. Choudhary, C. Maffeo, and A. Aksimentiev, Multi-resolution simulation of dna transport through large synthetic nanostructures, *Physical Chemistry Chemical Physics* **24**, 2706 (2022).
- [15] L. Peng, Y. Hao, R. Liu, Z. Zhao, and J. Li, Ionic current rectification properties of power-law fluids in a nanochannel with non-uniform surface charge density, *Physics of Fluids* **37** (2025).
- [16] S. K. Mehta and P. K. Mondal, Viscoelectric effect on the chemiosmotic flow in charged soft nanochannels, *Physics of Fluids* **35** (2023).
- [17] R. Rammoorthi and D. Mohanavel, Numerical simulation of an electromagnetic squeezing hybrid nanofluid flow through permeable plates with sensor monitoring system, *Physics of Fluids* **35** (2023).
- [18] S. Majhi and S. Bhattacharyya, Finite ion size effects on electrophoresis of a dielectric surfactant-laden droplet in a non-dilute electrolyte, *Applied Mathematical Modelling* **132**, 384 (2024).
- [19] S. Pennathur and J. G. Santiago, Electrokinetic transport in nanochannels. 2. experiments, *Analytical chemistry* **77**, 6782 (2005).
- [20] A. Siria, P. Poncharal, A.-L. Biance, R. Fulcrand, X. Blase, S. T. Purcell, and L. Bocquet, Giant osmotic energy conversion measured in a single transmembrane boron nitride nanotube, *Nature* **494**, 455 (2013).
- [21] I. Borukhov, D. Andelman, and H. Orland, Steric effects in electrolytes: A modified poisson-boltzmann equation, *Physical review letters* **79**, 435 (1997).
- [22] M. S. Kilic, M. Z. Bazant, and A. Ajdari, Steric effects in the dynamics of electrolytes at large applied voltages. ii. modified poisson-nernst-planck equations, *Physical Review E—Statistical, Nonlinear, and Soft Matter Physics* **75**, 021503 (2007).
- [23] D. Pandey and S. Bhattacharyya, Impact of finite ion size, born energy difference and dielectric decrement on the electroosmosis of multivalent ionic mixtures in a nanotube, *Colloids and Surfaces A: Physicochemical and Engineering Aspects* **610**, 125905 (2021).
- [24] D. Pandey and S. Bhattacharyya, Effects of membrane polarization, steric repulsion and ion-solvent interactions on electroosmosis through a conical nanopore, *Applied Mathematical Modelling* **111**, 471 (2022).
- [25] S. Sahu, B. Mondal, and S. Bhattacharyya, Ion steric interactions and electrostatic correlations on electro-osmotic flow in charged nanopores with multivalent electrolytes, *Physical Review Fluids* **9**, 074201 (2024).
- [26] D. R. Ladiges, A. Nonaka, K. Klymko, G. Moore, J. Bell, S. Carney, A. Garcia, S. Natesh, and A. Donev, Discrete ion stochastic continuum overdamped solvent algorithm for modeling electrolytes, *Physical Review Fluids* **6**, 044309 (2021).
- [27] L. Fumagalli, A. Esfandiari, R. Fabregas, S. Hu, P. Ares, A. Janardanan, Q. Yang, B. Radha, T. Taniguchi, K. Watanabe, *et al.*, Anomalous low dielectric constant of confined water, *Science* **360**, 1339 (2018).
- [28] J.-m. Zheng, W.-C. Chin, E. Khijniak, E. Khijniak Jr, and G. H. Pollack, Surfaces and interfacial water: evidence that hydrophilic surfaces have long-range impact, *Advances in colloid and interface science* **127**, 19 (2006).
- [29] A. Igljč, E. Gongadze, and K. Bohinc, Excluded volume effect and orientational ordering near charged surface in solution of ions and langevin dipoles, *Bioelectrochemistry* **79**, 223 (2010).
- [30] G. Monet, F. Bresme, A. Kornyshev, and H. Berthoumieux, Nonlocal dielectric response of water in nanoconfinement, *Physical Review Letters* **126**, 216001 (2021).

- [31] A. Abrashkin, D. Andelman, and H. Orland, Dipolar poisson-boltzmann equation: ions and dipoles close to charge interfaces, *Physical review letters* **99**, 077801 (2007).
- [32] P. Liu, X. Ji, and Z. Xu, Modified poisson–nernst–planck model with accurate coulomb correlation in variable media, *SIAM Journal on Applied Mathematics* **78**, 226 (2018).
- [33] J.-L. Liu and B. Eisenberg, Molecular mean-field theory of ionic solutions: A poisson–nernst–planck–bikerman model, *Entropy* **22**, 550 (2020).
- [34] S. Gui, B. Lu, and W. Yu, Ion transport in dipolar medium i: A local dielectric poisson–nernst–planck/poisson–boltzmann model, *SIAM Journal on Applied Mathematics* **84**, 2110 (2024).
- [35] K. Saurabh and M. Solovchuk, Mathematical and computational modeling of electrohydrodynamics through a nanochannel, *AIP Advances* **13** (2023).
- [36] E. N. D. C. Andrade and C. Dodd, The effect of an electric field on the viscosity of liquids, *Proceedings of the Royal Society of London. Series A. Mathematical and Physical Sciences* **187**, 296 (1946).
- [37] E. N. D. C. Andrade and C. Dodd, The effect of an electric field on the viscosity of liquids. ii, *Proceedings of the Royal Society of London. Series A. Mathematical and Physical Sciences* **204**, 449 (1951).
- [38] J. Lyklema and J. T. G. Overbeek, On the interpretation of electrokinetic potentials, *Journal of Colloid Science* **16**, 501 (1961).
- [39] R. J. Hunter and J. Leyendekkers, Viscoelectric coefficient for water, *Journal of the Chemical Society, Faraday Transactions 1: Physical Chemistry in Condensed Phases* **74**, 450 (1978).
- [40] D. Jin, Y. Hwang, L. Chai, N. Kampf, and J. Klein, Direct measurement of the viscoelectric effect in water, *Proceedings of the National Academy of Sciences* **119**, e2113690119 (2022).
- [41] W.-L. Hsu, H. Daiguji, D. E. Dunstan, M. R. Davidson, and D. J. Harvie, Electrokinetics of the silica and aqueous electrolyte solution interface: Viscoelectric effects, *Advances in Colloid and Interface Science* **234**, 108 (2016).
- [42] S. K. Mehta, G. Biswas, and P. K. Mondal, Arresting of viscoelectric effect modulated flow reduction in nanochannels with imposed temperature gradients, *Langmuir* **41**, 19754 (2025).
- [43] D. Mattia, H. Leese, and F. Calabrò, Electro-osmotic flow enhancement in carbon nanotube membranes, *Philosophical Transactions of the Royal Society A: Mathematical, Physical and Engineering Sciences* **374**, 20150268 (2016).
- [44] S. Sinha, L. Myers, and S. Das, Effect of solvent polarization on electroosmotic transport in a nanofluidic channel, *Microfluidics and Nanofluidics* **20**, 1 (2016).
- [45] J.-S. Sin, N.-H. Kim, C.-H. Kim, and Y.-M. Jang, Influence of solvent polarization and non-uniform ionic size on electrokinetic transport in a nanochannel, *Microfluidics and Nanofluidics* **22**, 1 (2018).
- [46] P. Srinivasula, Dipolar solvent corrections in nanopore electroosmotic flow with different surface electrostatic conditions, *Journal of Electrostatics* **138**, 104201 (2025).
- [47] G. Di Muccio, S. Gargano, D. F. Iacoviello, B. M. della Rocca, and M. Chinappi, Validity of approximated expressions for electro-osmotic flow in nanopores evaluated by continuum electrohydrodynamics and atomistic simulations, *Flow* **5**, E28 (2025).
- [48] G. Blankenburg, H. Hernández-Alpizar, L. Lesser-Rojas, and C.-F. Chou, Nanoscale ac electroosmotic flow and the frequency–size scaling observed beyond the charge relaxation regime, *Nano Letters* (2025).
- [49] Y. Niu and Y. Xie, Electrohydrodynamics of ionic-surfactant-covered liquid films in soft memristors, *Physical Review Fluids* **10**, 093702 (2025).
- [50] J. N. Israelachvili, *Intermolecular and surface forces* (Academic press, 2011).
- [51] M. S. Kilic, M. Z. Bazant, and A. Ajdari, Steric effects in the dynamics of electrolytes at large applied voltages. i. double-layer charging, *Physical Review E—Statistical, Nonlinear, and Soft Matter Physics* **75**, 021502 (2007).
- [52] E. Gongadze, U. van Rienen, V. Kralj-Iglič, and A. Iglič, Spatial variation of permittivity of an electrolyte solution in contact with a charged metal surface: a mini review, *Computer methods in biomechanics and biomedical engineering* **16**, 463 (2013).
- [53] A. Baer, Z. Miličević, D. M. Smith, and A.-S. Smith, Water in an electric field does not dance alone: The relation between equilibrium structure, time dependent viscosity and molecular motions, *Journal of molecular liquids* **282**, 303 (2019).
- [54] M. Duan, L. Xu, J. Chen, and G. Chen, Non-monotonic salt dependence of electro-osmotic flow in ph-regulated nanochannels, *Journal of Fluid Mechanics* **1007**, R2 (2025).
- [55] D. Saville, Electrohydrodynamics: the taylor-melcher leaky dielectric model, *Annual review of fluid mechanics* **29**, 27 (1997).
- [56] M. Z. Bazant, K. Thornton, and A. Ajdari, Diffuse-charge dynamics in electrochemical systems, *Physical Review E—Statistical, Nonlinear, and Soft Matter Physics* **70**, 021506 (2004).
- [57] X. Zhao, Y. Zhang, and G. Qing, Nanopore toward genuine single-molecule sensing: Molecular ping-pong technology, *Nano Letters* **25**, 3692 (2025).
- [58] G. Laucirica, Y. Toum-Terrones, V. Cayón, M. Toimil-Molares, O. Azzaroni, and W. A. Marmisollé, Advances in nanofluidic field-effect transistors: external voltage-controlled solid-state nanochannels for stimulus-responsive ion transport and beyond, *Physical Chemistry Chemical Physics* **26**, 10471 (2024).